Applied Catalysis B: Environmental 224 (2018) 305–309

Contents lists available at ScienceDirect

Applied Catalysis B: Environmental

journal homepage: www.elsevier.com/locate/apcatb

Research Paper

Operando SERS self-monitoring photocatalytic oxidation of aminophenol on TiO_2 semiconductor

Xuefeng Yan, Yin Xu, Baozhu Tian, Juying Lei, Jinlong Zhang, Lingzhi Wang*

Key Laboratory for Advanced Materials and Institute of Fine Chemicals, East China University of Science and Technology, Meilong Road 130, Xuhui District, Shanghai, 200237, PR China

ARTICLE INFO

Keywords:
TiO_2
SERS
Photocatalysis
Operando

ABSTRACT

The utilization of the fingerprint spectrum for the operando monitoring of a photocatalytic process is extremely desired to accurately understand the reaction mechanism but long remains challenging. Here, ordered macroporous TiO_2 that is concomitantly photocatalytically active and high surface-enhanced Raman scattering (SERS) sensitive was unprecedentedly employed to self-track the photocatalytic reaction using the oxidation of *p*-aminothiophenol (PATP) as the model. The photocatalytic degradation under 532 nm laser irradiation initiated from the formation of the azo compound was explicitly revealed by finely resolved SERS spectra. More importantly, the decomposition rates of different bonds including N=N, C–S and C–C were respectively determined, following a first-order kinetics process with the rates in the range of 2.1–2.7 × 10^{-3} s^{-1}. Meanwhile, this self-monitoring strategy also provides an opportunity for gaining an insight into the effect of photothermal catalysis on selective formation of the azo compound.

1. Introduction

A highly effective photocatalytic system for the controllable organic synthesis using sunlight as the energy source has become one of the keys to realizing a sustainable society [1–3]. Unfortunately, the photocatalytic technology using radicals of hole, electron and O-containing species with high oxidative potentials easily causes non-selective degradation of organics with poor controllability [4–6]. An elaborately designed structure often fails to deliver expected selective performance. Only few photocatalytic reaction models have exhibited reasonable selectivity. Thereby, an *in situ* and real-time monitoring technology for the photocatalytic process is urgently needed to well reveal the reaction path and finally achieve a rational structure design [7–11]. Fluorescence spectroscopy and ESR are two popular means for the real-time exploration of the relation between structure and activity [12–14]. The main problem of these analysis techniques is the dependence on the external label molecules, which are incapable of acquiring information about the adsorption and transformation of the reactant molecules on the surface of semiconductor.

Regarding the reaction tracking, the priority of Raman technology based on the molecular vibration and rotation lies in the fingerprint spectra interference-free from water [15,16]. However, Raman spectroscopy usually gives rise to strong signals of inorganic catalyst instead of surface chemical probes, preventing it from the application in tracing the transformation path of the surficial species. In contrast, SERS commonly shows superior surface sensitivity to adsorbed molecules, which has proven a strong technique for rapid and sensitive tracing of surface plasmon resonance (SPR) reactions on noble metal substrates such as Au and Ag [17–22]. Recently, the reaction kinetics of SPR reaction has also been successfully determined through SERS [23]. Semiconductors including TiO_2, Cu_2O, MoO_{3-x} have also proven to be SERS active [24–30]. It is desirable to *in situ* and real-time (operando) reveal the interfacial information between semiconductor and surficial reactants through SERS, which is extremely significant for guiding the photocatalyst design. However, restricted by the low sensitivity, there is no study about SERS self-tracking of the photocatalytic process on semiconductor. Recently, TiO_2 with cavitary structure has been revealed to be highly SERS sensitive with an enhance factor over 10^4 due to the improved light scattering efficiency, which provides possibility for the operando self-monitoring of the photocatalysis reaction [31,32].

Here, benefitting from the striking SERS activity of ordered macroporous TiO_2 inverse opal (IO) independent on the excitation wavelength from UV to near infrared region [30,32–34], fingerprint-tracking of the photocatalytic oxidation of PATP on TiO_2 has been achieved for the first time. The immediate transformation of PATP to the azo compound, 4, 4'-dimercaptoazobenzene (DMAB) followed by the continuous decomposition of the functional groups under 532 nm irradiation has been operando revealed. The reaction kinetics of different

* Corresponding author.
E-mail address: wlz@ecust.edu.cn (L. Wang).

http://dx.doi.org/10.1016/j.apcatb.2017.10.009
Received 9 August 2017; Received in revised form 27 September 2017; Accepted 6 October 2017
Available online 13 October 2017

functional groups was determined. Besides, the contribution of photothermal catalysis to the formation of DMAB has also been successfully identified.

2. Experimental section

2.1. Chemical

Acetylacetone, methanol, HCl, ammonium oxalate (AO) and t-butanol (TBA) were purchased from Shanghai Lingfeng Chemical Reagent Co. Ltd without further purification. $K_2Cr_2O_7$ and ethanol were purchased from Shanghai Chemical Reagent. Titanium isopropoxide (TTIP) and *p*-aminothiophenol were purchased from Aladdin. P25 was purchased from Evonik Industries AG. Ultrapure water (=18.0 MΩ) purified using the Milipore Milli-Q gradient system.

2.2. Preparation of PS colloidal crystal template arrays

400 μL of polystyrene (PS) suspension was ultrasonically dispersed into 25 mL ultrapure water, and a glass slide was vertically placed in the beaker. The beaker was kept into 70 °C oven until the water was completely evaporated.

2.3. Preparation of TiO_2 inverse opal substrates

TTIP solution was used as precursor and prepared as follows. 5.6 mL TTIP, 45 mL ethanol and 1 mL acetylacetone were mixed and stirred. After that, 0.85 mL hydrochloric acid and 4.6 mL H_2O were added into the solution. After stirring for 2 h, 100 μL solution was spin-coated on the PS template films, which was then calcined at 450 °C for 2 h (heating rate was 2 °C/min).

2.4. Characterization

Scanning electron microscopy (SEM) analysis was performed using a TESCAN nova III scanning electron microscope. Transmission electron microscopy (TEM) analysis was performed using a JEOL 2100 LaB6 TEM, at a 200 kV accelerating voltage. Raman spectra were recorded on a Renishaw inVia-Reflex Raman microprobe system equipped with Peltier charge-coupled device (CCD) detectors and a Leica microscope. Spectra were collected from the film with an accumulation time of 10 s. Lasers with wavelength of 532 nm and 785 nm were used as the excitation light source, and a 50× objective with a numerical aperture (NA) of 0.75 was used to get the laser spot diameter of ~1 μm. By utilizing the Barrett–Joyner–Halenda (BJH) model, the pore volumes and pore size distributions were got from the adsorption branches of isotherms. X-ray diffraction (XRD) patterns of the samples were recorded on a Rigaku D/MAX-2550 diffractometer using Cu Kα radiation of wavelength 1.5406 Å, typically run at a voltage of 40 kV and current of 100 mA. UV–vis absorbance spectra were achieved by using a Scan UV–vis spectrophotometer (Shimadzu UV-2450).

3. Result and discussion

For the SERS monitoring of the photocatalysis, TiO_2 IO was first fabricated using polystyrene (PS) as a hard template [35]. Scanning electron microscopy (SEM) images show ordered macroporous microarray with a cavity size of ca. 250 nm (Fig. 1). XRD pattern shows typical diffraction peaks at 25.3, 37.8, 48.0, 53.9 and 55.0°, indicative of an anatase phase (Fig. S1). The loading density of PATP was calculated to be ca. 10^{19} molecules/m^2 based on the specific surface area (54.8 m^2/g, Fig. S2). The maximum molecular layers were determined as ca. 2.8 by assuming a parallel alignment of the benzene ring (ca. 0.6 nm) on the substrate. Two lasers with wavelengths of 785 and 532 nm were adopted to understand the photocatalytic conversion of PATP. For TiO_2 IO without PATP, strong peaks can be clearly observed at 146, 399, 519 and 640 cm^{-1}, which are ascribed to the E_g (symmetric stretching vibration), B_{1g} (symmetric bending vibration), A_{1g} (antisymmetric bending vibration), and E_g modes of anatase TiO_2 (Fig. S3), in line with the result from XRD analysis [36,37]. Under 785 nm irradiation (Fig. 2a), strong peaks are observed at 1089 and 1593 cm^{-1} from TiO_2 IO covered with PATP, which are assigned to the vibration stretching modes of C-S ($\nu_{C\text{-}S}$) and C-C ($\nu_{C\text{-}C}$), respectively. The peak at 475 cm^{-1} is attributed to the out-of-plane bending vibration of the aromatic ring (γ_{CCC}). In contrast, under the irradiation of 532 nm laser (Fig. 2b), the peak at 475 cm^{-1} disappears, accompanied by the appearance of new peaks at 1145 cm^{-1} due to β_{CH}, 1390 and 1437 cm^{-1} from $\nu_{N=N}$, suggesting the formation of the azo compound DMAB. In contrast, PATP molecules dispersed on commercial P25 show weak signals no matter under the irradiation of 532 or 785 nm laser (red line). Moreover, when the UV laser is used (365 nm), only a broad amorphous peak around 1700 cm^{-1} can be observed (Fig. S4), which actually originates from the glass slide.

Furthermore, the effect of the irradiation time was investigated with 532 nm laser to more deeply understand the oxidation process of PATP. It is obvious the intensity of characteristic $\nu_{N=N}$ peak (1437 cm^{-1}) gradually decreases within 15 min at a fixed interval (5 min) and laser power (5.0 mW, Fig. 3a). Meanwhile, peaks of $\nu_{C\text{-}S}$ (1089 cm^{-1}) and $\nu_{C\text{-}C}$ (1593 cm^{-1}) show the same tendency. In contrast, the peak intensity related to TiO_2 substrate remain unchanged (Fig. S5), demonstrating the stability of the SERS substrate during the long-time irradiation. On the other hand, no variation of PATP on glass slide is observed after an irradiation for 15 min (Fig. S6). The above results demonstrate the formation of DMAB and the subsequent weakening of the SERS bands are both attributed to the photocatalytic transformation instead of photodecomposition or loss of SERS activity suffered from a long-time laser irradiation. To verify the above assumption, the photocatalytic conversion of PATP by TiO_2 was investigated on commercial P25 and analyzed by commonly used UV–vis absorption spectroscopy. Under UV light irradiation, the peak centered at ca. 250 nm gradually decreases, which is commonly deemed as a result of photocatalytic degradation (Fig. S7) and accordant with the fact that no Raman signal is observed under UV laser irradiation (Fig. S4). The decrease of the peak at 250 nm slows down under the visible-light irradiation, accompanied by the appearance of a distinct tail above 400 nm at 12 h (Fig. S8a). High performance liquid chromatography (HPLC) for the product after 12 h reaction presents complicated peaks besides the peak at 12 min attributed to the original PATP (Fig. S8b). The electrospray ionization mass spectrometry (ESI–MS) indicates besides products from the ring-opening of PATP, an azo compound of DMAB is formed (Fig. S8c). The combinational analyses from UV–vis absorption spectroscopy, HPLC and ESI–MS verify the photocatalytic transformation of PATP to DMAB and the further degradation, demonstrating the feasibility of SERS for operando self-monitoring of the photocatalytic process. The quicker reaction rate observed from SERS should be attributed to the extremely low reactant concentration and high incident photon density.

Owing to the distinct SERS signal during the irradiation process, it is possible to determine the reaction kinetics by collecting all the data at the same location, which has recently been achieved on noble metal SERS substrate [23]. The SERS spectra were then continuously recorded by setting the data-collecting time as 30 s, which were all processed using the normalized vibration peak intensity of TiO_2 at 146 cm^{-1} as an internal control because of the stability of the substrate during the long-time irradiation. According to the maximum molecular layers (2.8) calculated by assuming a parallel alignment of PATP on the surface of TiO_2 IO, the chemisorbed PATP through a non-parallel complexing between −SH and Ti is thereafter approximately considered as monolayer [6,21]. The integrated band intensity of different functional groups (denoted as I_t) was proportional to the surface coverage percentage, θ, of PATP, so is the corresponding chemical bond (i.e., $\theta_{[bond]}(t) = I_t/I_0$, where I_0 refers to the initial intensity at full coverage). The equation of turnover frequency (TOF) can be expressed as:

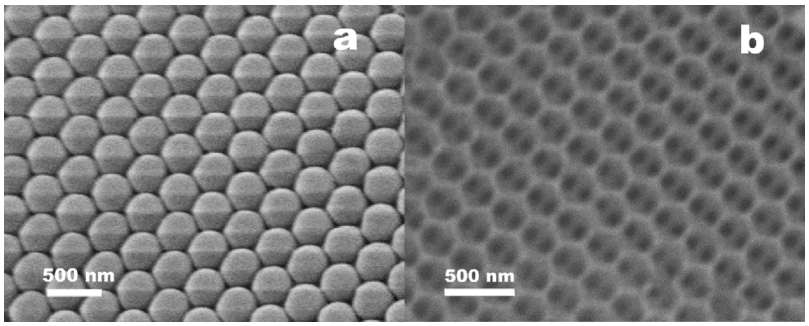

Fig. 1. SEM images of PS sphere microarray (a) and TiO_2 inverse opal (b).

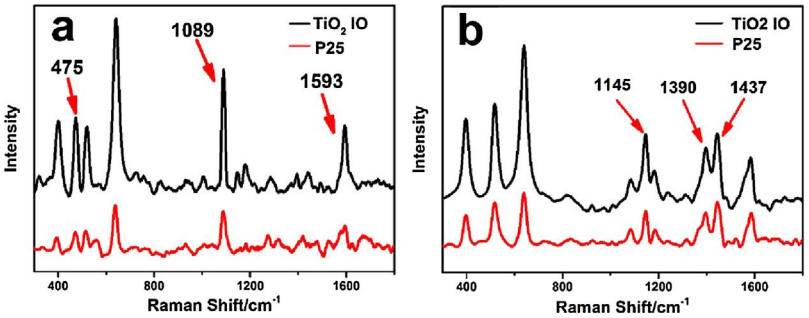

Fig. 2. SERS spectra of PATP on TiO_2 IO (black) and P25 (red) substrates under the irradiation of 785 nm (a) and 532 nm (b) lasers. The laser power is 5 mW. (For interpretation of the references to colour in this figure legend, the reader is referred to the web version of this article.)

$$\mathrm{TOF} = -\frac{\partial\theta_{[bond]}}{\partial t} = k\theta_{[bond]}(t)^n \quad (1)$$

where n is the reaction order of PATP. To simplify the equation, logarithm was employed and Eq. (1) can be simplified as follows:

$$ln\left(-\frac{\partial\theta_{[bond]}}{\partial t}\right) = lnk + nln(I_t/I_0) \quad (2)$$

Hence, both the reaction order and the rate constant, k, can be calculated on the basis of the (I_t/I_0) evolution diagram. Here, using the

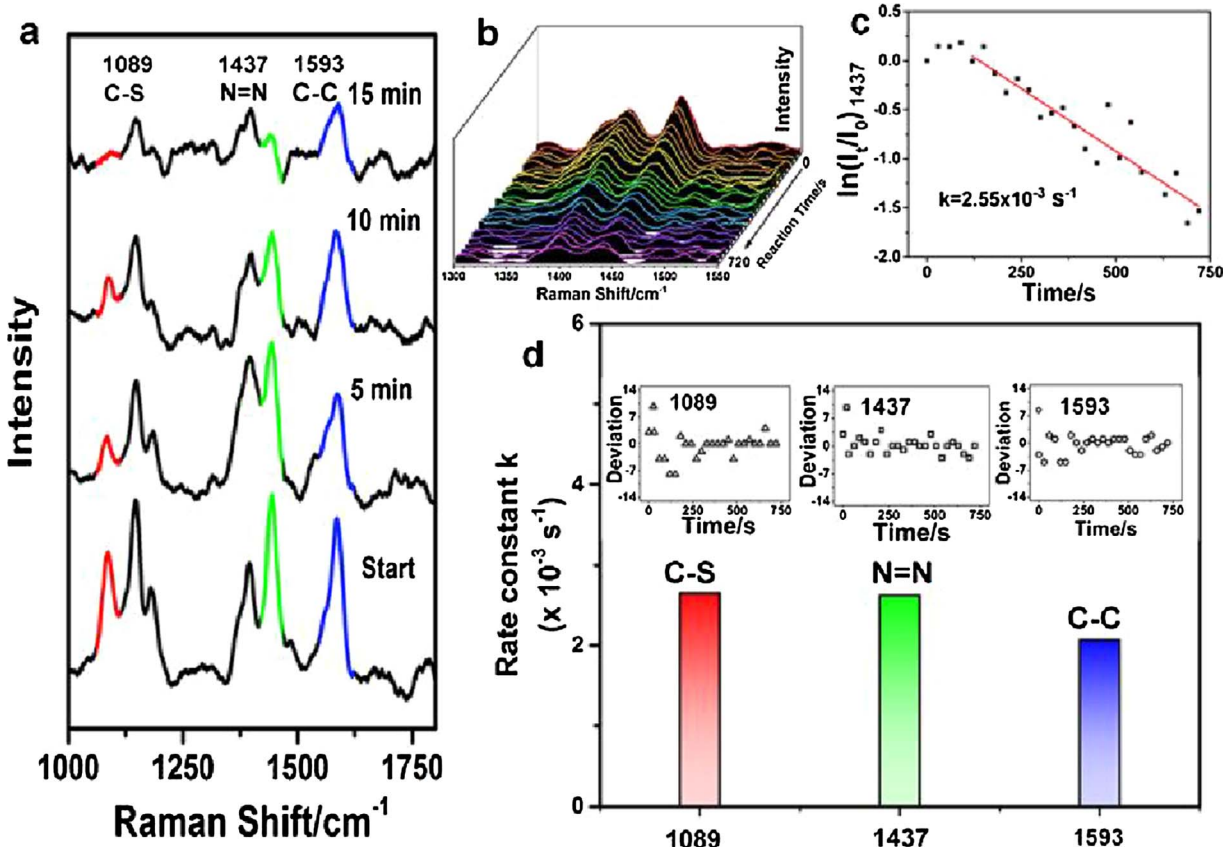

Fig. 3. (a) SERS spectra of PATP on TiO_2 IO under the irradiation of 532 nm laser for 15 min with a time interval of 5 min; (b) Evolution of $\nu_{N=N}$ peak recorded with a time interval of 30 s; (c) The logarithm of $(I_t/I_0)_{1437}$ processed using the normalized vibration peak intensity of TiO_2 at 146 cm^{-1} as an internal control; (d) Reaction rate constants for the cleavage of C-S, N═N and C−C bonds under the long-time irradiation of 532 nm laser with a power of 5.0 mW and the corresponding wavenumber deviation collected at different time (Inset).

evolution of characteristic $\nu_{N=N}$ peak of DMAB as a representative (Fig. 3b), the $\ln(I_t/I_0)$ shows an upward trend within the first 90 s (Fig. 3c), which is followed by a continuous decrease. We suggested the decrease caused by the bond cleavage belongs to the first-order kinetics for its linear regression (Fig. S9). Hence, Eq. (3) becomes

$$ln(I_t/I_0) = -kt \quad (3)$$

A degradation rate constant of k = 2.55 × 10^{-3} s^{-1} can thus be readily derived from the linearly fitted slope of the $\ln(I_t/I_0)$ ~ t plot (Fig. 3c). The formation rate constant of N=N bond within the first 90 s is also determined (2.37 × 10^{-3} s^{-1}, Fig. S10), indicating the immediate formation of DMAB followed by a continuous degradation. In a similar way, the TOF of C–S and C–C bond can also be calculated based on the peak at 1089 and 1593 cm^{-1}, which have reaction rate constants of 2.65 × 10^{-3} $s^{-1}$and 2.1 × 10^{-3} s^{-1} (Fig. 3d), respectively. Moreover, all the bands show a standard deviation of the wavenumber within ± 10 cm^{-1} (Inset, Fig. 3d), demonstrating a sound reliability for the data-collecting at a fixed area.

To exclude the possible altering of the reaction path by the high-energy laser irradiation compared with the photoreaction carried out under simulated solar light with lower photon density, a much weaker laser power (0.25 mW) was used, which results in a similar SERS spectrum with $\nu_{N=N}$ peak characteristic of DMAB, although the peak intensity significantly decreases (Fig. S11). Therefore, it is undoubted that under the visible light irradiation, PATP first transforms into DMAB, which further undergoes versatile bond cleavages at different rates. The above results well demonstrate the robustness of the operando SERS from TiO_2 IO for the self-tracking of photocatalytic reaction due to the avoiding of tedious purification and separation process for different products.

Moreover, it is noted that in the case of 785 nm laser irradiation, although the variation of laser power in the range of 0.25–5 mW does not cause any change of PATP (Fig. S12), small peaks attributed to DMAB are surprisingly observed at 1140, 1395 and 1437 cm^{-1} after 40 min irradiation of 785 nm laser with a power of 5 mW (Fig. 4a). According to the UV–vis diffuse reflectance spectrum of TiO_2-PATP film, no absorption band can be observed in the near-IR range (Fig. S13), which excludes the possible photo-sensitization effect during the photocatalytic process. Therefore, this unusual signal should be attributed to the hot effect of laser due to the long-time irradiation. The reaction constant calculated from N=N bond is about 5.43 × 10^{-4} s^{-1} (Fig. 4b), which is much slower than that of the photocatalytic process.

Finally, versatile radical capturers were used to reveal the active species for the initial photocatalytic conversion of PATP to DMAB (Fig. 5). First, $K_2Cr_2O_7$ as an electron capturer was added, which accelerates the photocatalytic oxidation of PATP to DMAB according to the improved peak intensity of azo group (red line). In contrast, when

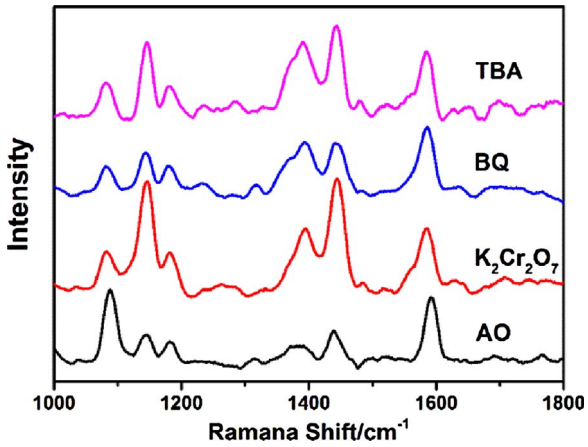

Fig. 5. SERS spectra of PATP on TiO_2 IO substrate by adding different sacrificial agents.

the ammonium oxalate (AO) is adopted as the capturer for holes, the conversion of PATP to DMAB was completely suppressed. Meanwhile, the addition of *tert*-butanol (TBA) as a ·OH capturer or *p*-benzoquinone (BQ) as a $\cdot O_2^-$ capturer seems to be ineffective in altering the reaction process, excluding the possible effect of ·OH and $\cdot O_2^-$ on the oxidation of PATP. Since PATP actually has a weak absorption in the visible light range of 400–600 nm besides the main peak in the UV range (Fig. S13), the electron can be excited from the HOMO to LUMO of PATP under the irradiation of 532 nm laser. The excited electron may transfer from PATP to the conduction band of TiO_2. The depressed oxidation of PATP with AO suggests the remained hole in the HOMO of PATP should be responsible for the photocatalytic oxidation. Thereby, the enhanced oxidation of PATP in the presence of electron sacrificing agent of $K_2Cr_2O_7$ should be attributed to the accelerated separation of electron-hole pair. On the other hand, the electrons in the valence band of TiO_2 can be directly excited to the conduction band when the ultraviolet laser was used, leading to the separation of holes and electron. This process is subsequently followed by the generation of radicals of $\cdot O_2^-$ and ·OH with non-selective oxidation ability, which finally cause the decomposition of PATP according to the decreased SERS signals. Therefore, the bond cleavage of DMAB upon the long-time irradiation of 532 nm laser should be attributed to the overmuch accumulated holes, which gradually transform to ·OH with non-selective oxidation ability.

4. Conclusion

In conclusion, we demonstrate the self-monitoring of photocatalytic reaction on IO structured TiO_2 through the cavity-based SERS using

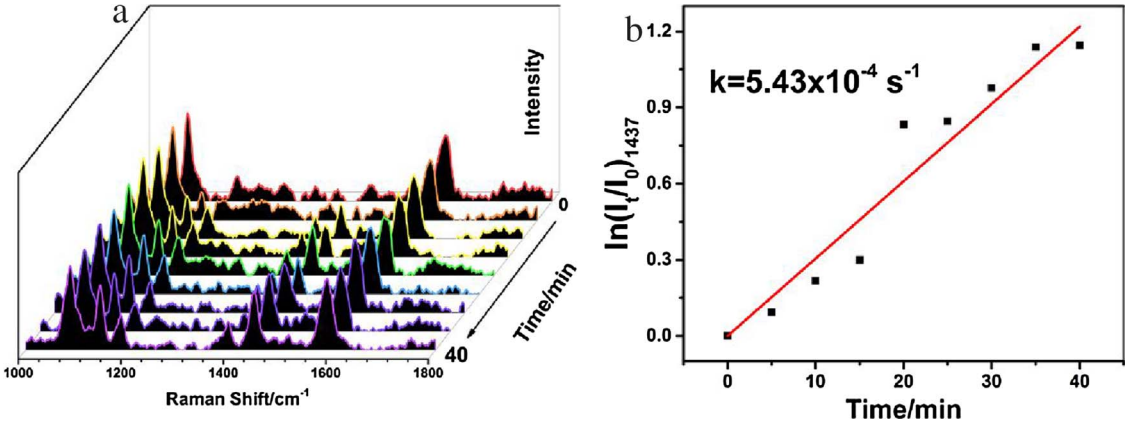

Fig. 4. (a) Evolution of $\nu_{N=N}$ peak recorded with a time interval of 30 s; (b) The logarithm of $(I_t/I_0)_{1437}$ processed using the normalized vibration peak intensity of TiO_2 at 146 cm^{-1} as an internal control.

PATP as the probe for the first time. The oxidation of PATP to DMAB and the subsequent decomposition under visible laser irradiation have been in-situ and real-time identified with the fingerprint SERS spectra through the elaborate study about the effect of laser wavelength, power and irradiation time. The contribution of sensitization and photothermal effect to the oxidation of PATP to DMAB was verified. The decomposition of as-formed DMAB under 532 nm laser irradiation was operando followed and the kinetics rates of different bonds were successfully determined as a benefit of distinct SERS signal. This strategy provides a brand-new means to track the photocatalytic process on the surface of semiconductor and is expected to offer direct insight into the photocatalytic mechanism regarding the prosperous development of SERS imaging technology.

Funding

This work is supported by the National Natural Science Foundation of China [21673073, 21677048, U1407102 and 21377038], the National Basic Research Program of China [973 Program, 2013CB632403], the Science and Technology Commission of Shanghai Municipality [14230710500, 14ZR1410700 and 16JC1401400] and the Fundamental Research Funds for the Central Universities, PetroChina Innovation Foundation [2015D-5006-0402] and the Fundamental Research Funds for the Central Universities [222201717003].

Acknowledgment

Xuefeng Yan and Yin Xu have contributed equally to this paper.

Appendix A. Supplementary data

Supplementary data associated with this article can be found, in the online version, at http://dx.doi.org/10.1016/j.apcatb.2017.10.009.

References

[1] X. Chen, Y. Li, X. Pan, D. Cortie, X. Huang, Z. Yi, Photocatalytic oxidation of methane over silver decorated zinc oxide nanocatalysts, Nat. Commun. 7 (2016) 12273.
[2] B. Cao, G. Li, H. Li, Hollow spherical RuO_2@TiO_2@Pt bifunctional photocatalyst for coupled H_2 production and pollutant degradation, Appl. Catal. B 194 (2016) 42–49.
[3] L. Jiang, H. Yu, L. Shi, Y. Zhao, Z. Wang, M. Zhang, S. Yuan, Optical band structure and photogenerated carriers transfer dynamics in FTO/TiO_2 heterojunction photocatalysts, Appl. Catal. B 199 (2016) 224–229.
[4] W. He, H.K. Kim, W.G. Wamer, D. Melka, J.H. Callahan, J.J. Yin, Photogenerated charge carriers and reactive oxygen species in ZnO/Au hybrid nanostructures with enhanced photocatalytic and antibacterial activity, J. Am. Chem. Soc. 136 (2014) 750–757.
[5] M. Setvin, U. Aschauer, J. Hulva, T. Simschitz, B. Daniel, M. Schmid, A. Selloni, U. Diebold, Following the reduction of oxygen on TiO_2 anatase (101) step by step, J. Am. Chem. Soc. 138 (2016) 9565–9571.
[6] X. Yan, L. Wang, X. Tan, B. Tian, J. Zhang, Surface-enhanced Raman spectroscopy assisted by radical capturer for tracking of plasmon-driven redox reaction, Sci. Rep. 6 (2016) 30193.
[7] L. Shi, C. Jing, W. Ma, D.W. Li, J.E. Halls, F. Marken, Y.T. Long, Plasmon resonance scattering spectroscopy at the single-nanoparticle level: real-time monitoring of a click reaction, Angew. Chem. Int. Ed. 52 (2013) 6011–6014.
[8] H. Imai, K. Izumi, M. Matsumoto, Y. Kubo, K. Kato, Y. Imai, In situ and real-time monitoring of oxide growth in a few monolayers at surfaces of platinum nanoparticles in aqueous media, J. Am. Chem. Soc. 131 (2009) 6293–6300.
[9] B. Hulsken, R. Van Hameren, J.W. Gerritsen, T. Khoury, P. Thordarson, M.J. Crossley, A.E. Rowan, R.J. Nolte, J.A. Elemans, S. Speller, Real-time single-molecule imaging of oxidation catalysis at a liquid-solid interface, Nat. Nanotechnol. 2 (2007) 285–289.
[10] H. Shi, R.T. Kwok, J. Liu, B. Xing, B.Z. Tang, B. Liu, Real-time monitoring of cell apoptosis and drug screening using fluorescent light-up probe with aggregation-induced emission characteristics, J. Am. Chem. Soc. 134 (2012) 17972–17981.
[11] Y.S. Jiang, B. Li, J.N. Milligan, S. Bhadra, A.D. Ellington, Real-time detection of isothermal amplification reactions with thermostable catalytic hairpin assembly, J. Am. Chem. Soc. 135 (2013) 7430–7433.
[12] A.D. McFarland, R.P. Van Duyne, Single silver nanoparticles as real-time optical sensors with zeptomole sensitivity, Nano Lett. 3 (2003) 1057–1062.
[13] M. Sathiya, J.B. Leriche, E. Salager, D. Gourier, J.M. Tarascon, H. Vezin, Electron paramagnetic resonance imaging for real-time monitoring of Li-ion batteries, Nat. Commun. 6 (2015) 6276.
[14] Y. Jiang, M. Wang, J. Hardie, G.Y. Tonga, M. Ray, Q. Xu, V.M. Rotello, Chemically engineered nanoparticle-protein interface for real-time cellular oxidative stress monitoring, Small 12 (2016) 3775–3779.
[15] S.-Y. Ding, J. Yi, J.-F. Li, B. Ren, D.-Y. Wu, R. Panneerselvam, Z.-Q. Tian, Nanostructure-based plasmon-enhanced Raman spectroscopy for surface analysis of materials, Nat. Rev. Mater. 1 (2016) 16021.
[16] K. Kim, S. Coh, L.Z. Tan, W. Regan, J.M. Yuk, E. Chatterjee, M.F. Crommie, M.L. Cohen, S.G. Louie, A. Zettl, Raman spectroscopy study of rotated double-layer graphene: misorientation-angle dependence of electronic structure, Phys. Rev. Lett 108 (2012) 246103.
[17] W. Shen, X. Lin, C. Jiang, C. Li, H. Lin, J. Huang, S. Wang, G. Liu, X. Yan, Q. Zhong, B. Ren, Reliable quantitative SERS analysis facilitated by core-shell nanoparticles with embedded internal standards, Angew. Chem. Int. Ed. 54 (2015) 7308–7312.
[18] Z. Zhang, T. Deckert-Gaudig, P. Singh, V. Deckert, Single molecule level plasmonic catalysis—a dilution study of p-nitrothiophenol on gold dimers, Chem. Commun. 51 (2015) 3069–3072.
[19] W. Xie, C. Herrmann, K. Kompe, M. Haase, S. Schlucker, Synthesis of bifunctional Au/Pt/Au core/shell nanoraspberries for in situ SERS monitoring of platinum-catalyzed reactions, J. Am. Chem. Soc. 133 (2011) 19302–19305.
[20] W. Xie, B. Walkenfort, S. Schlucker, Label-free SERS monitoring of chemical reactions catalyzed by small gold nanoparticles using 3D plasmonic superstructures, J. Am. Chem. Soc. 135 (2013) 1657–1660.
[21] D. Qi, X. Yan, L. Wang, J. Zhang, Plasmon-free SERS self-monitoring of catalysis reaction on Au nanoclusters/TiO_2 photonic microarray, Chem. Commun. 51 (2015) 8813–8816.
[22] J.F. Li, Y.F. Huang, Y. Ding, Z.L. Yang, S.B. Li, X.S. Zhou, F.R. Fan, W. Zhang, Z.Y. Zhou, D.Y. Wu, B. Ren, Z.L. Wang, Z.Q. Tian, Shell-isolated nanoparticle-enhanced Raman spectroscopy, Nature 464 (2010) 392–395.
[23] J. Huang, Y. Zhu, M. Lin, Q. Wang, L. Zhao, Y. Yang, K.X. Yao, Y. Han, Site-specific growth of Au-Pd alloy horns on Au nanorods: a platform for highly sensitive monitoring of catalytic reactions by surface enhancement Raman spectroscopy, J. Am. Chem. Soc. 135 (2013) 8552–8561.
[24] X. Tan, L. Wang, C. Cheng, X. Yan, B. Shen, J. Zhang, Plasmonic MoO3-x@MoO3 nanosheets for highly sensitive SERS detection through nanoshell-isolated electromagnetic enhancement, Chem. Commun. 52 (2016) 2893–2896.
[25] J. Wang, R.A. Ando, P.H. Camargo, Controlling the selectivity of the surface plasmon resonance mediated oxidation of p-aminothiophenol on Au nanoparticles by charge transfer from UV-excited TiO_2, Angew. Chem. Int. Ed. 54 (2015) 6909–6912.
[26] W. Ji, Y. Wang, I. Tanabe, X.X. Han, B. Zhao, Y. Ozaki, Semiconductor-driven turn-off surface-enhanced Raman scattering spectroscopy: application in selective determination of chromium(VI) in water, Chem. Sci. 6 (2015) 342–348.
[27] W. Ji, W. Song, I. Tanabe, Y. Wang, B. Zhao, Y. Ozaki, Semiconductor-enhanced Raman scattering for highly robust SERS sensing: the case of phosphate analysis, Chem. Commun. 51 (2015) 7641–7644.
[28] W. Ji, Y. Kitahama, X. Han, X. Xue, Y. Ozaki, B. Zhao, pH-dependent SERS by semiconductor-controlled charge-transfer contribution, J. Phys. Chem. C 116 (2012) 24829–24836.
[29] J. Lin, Y. Shang, X. Li, J. Yu, X. Wang, L. Guo, Ultrasensitive SERS detection by defect engineering on single Cu_2O superstructure particle, Adv. Mater. 29 (2017).
[30] I. Alessandri, Enhancing Raman scattering without plasmons: unprecedented sensitivity achieved by TiO_2 shell-based resonators, J. Am. Chem. Soc. 135 (2013) 5541–5544.
[31] D. Qi, L. Lu, L. Wang, J. Zhang, Improved SERS sensitivity on plasmon-free TiO_2 photonic microarray by enhancing light-matter coupling, J. Am. Chem. Soc. 136 (2014) 9886–9889.
[32] X. Li, H. Hu, D. Li, Z. Shen, Q. Xiong, S. Li, H.J. Fan, Ordered array of gold semishells on TiO_2 spheres: an ultrasensitive and recyclable SERS substrate, ACS Appl. Mater. Interfaces 4 (2012) 2180–2185.
[33] I. Alessandri, M. Ferroni, Exploiting optothermal conversion for nanofabrication: site-selective generation of Au/TiO2 inverse opals, J. Mater. Chem. 19 (2009) 7990.
[34] M. Liu, X. Li, S.K. Karuturi, A.I. Tok, H.J. Fan, Atomic layer deposition for nanofabrication and interface engineering, Nanoscale 4 (2012) 1522–1528.
[35] D. Qi, L. Lu, L. Wang, J. Zhang, Improved SERS sensitivity on plasmon-free TiO(2) photonic microarray by enhancing light-matter coupling, J. Am. Chem. Soc. 136 (2014) 9886–9889.
[36] J. Zhang, M. Li, Z. Feng, J. Chen, C. Li, UV Raman spectroscopic study on TiO_2. I. Phase transformation at the surface and in the bulk, J. Phys. Chem. B 110 (2006) 927–935.
[37] F. Tian, Y. Zhang, J. Zhang, C. Pan, Raman spectroscopy a new approach to measure the percentage of anatase TiO_2 exposed (001) facets, J. Phys. Chem. C 116 (2012) 7515–7519.